Spectral Estimation-based OFDM Radar Algorithms for IEEE 802.11a Signals

Martin Braun, Manuel Fuhr and Friedrich K. Jondral
Communications Engineering Lab, Karlsruhe Institute of Technology (KIT), Germany
martin.braun@kit.edu, manuel.fuhr@student.kit.edu, friedrich.jondral@kit.edu

***Abstract*—Recently, OFDM radar has gained attention as new algorithms for range and Doppler estimation specific to OFDM signals have been developed. The major advantage of OFDM is that it is both well-suited for radar processing as well as being suitable for communication.**

In previous work, we have proposed parametrizations for OFDM signals which suit the radar problem well. However, the proposed algorithms are independent of the OFDM signal parametrization, and it is therefore interesting to see how well they work with other, more commonly available signals. For this paper, we examine a common type of signal–OFDM signals according to the IEEE 802.11a standard–and determine how they could be used in a radar application.

***Index Terms*—OFDM, Radar, Car-to-car**

I. Introduction

For the joint usage of signals for both radar and communications, *OFDM radar* has been recently proposed by Sturm et al. [1], [2], [3]. The principle is simple: packets of data are modulated into an OFDM signal and then transmitted. While any receiver within transmission range can detect and demodulate these packets, the signal is also backscattered by objects obstructing the signal's wavefront. If the transmitting node is equipped with a receiver front-end, it can receive the backscattered signals and determine range and relative velocity of the reflecting objects, thereby creating a *radar image*.

A major difference of the aforementioned radar approach, dubbed *spectral estimation based OFDM radar*, to other suggestions on how to implement OFDM radar (e.g. in [4]) is the way the radar images are calculated: By simple transformations of the received signal, the detection of targets and the identification of their respective range and relative velocity becomes a straightforward problem of spectral estimation (see the following section for details). More importantly, the radar imaging works independently of the information transmitted. This makes spectral estimation based OFDM radar the perfect choice for the combination of communication and radar sensor networks.

In our previous work, we have analyzed this concept in great depth, including the parametrization of the OFDM signals [5], [6]. The focus was always on vehicular applications, trying to adapt the OFDM radar system such that cars could perform both radar sensing and communication with a single waveform; such a system could be used to improve road safety.

However, this is not the only application for OFDM radar. Its main advantage is the fact that the signals used for the radar imaging are regular OFDM signals, as opposed to more common radar systems, which use frequency-modulated continuous wave (FMCW) or pulse signals. Therefore, anywhere OFDM signals are used, a potential primary active radar system is available at zero additional spectrum usage.

In this paper, we will discuss the possibility to add a receiver to a IEEE 802.11a wi-fi system, one of the most common systems to use OFDM. This will require the transceiver to receive simultaneously while transmitting, as well as some additional signal processing, thereby adding radar functionality to a wi-fi access point. Such a setup becomes particularly useful if the receiving antenna has some kind of directivity, as this also allows us to estimate the angle at which a reflecting object is to the receiver.

A potential application is, e.g., the detection of moving objects in locations which are illuminated by such access points. Given that even some vehicles are nowadays equipped with wi-fi, this could even be used as an additional radar system in vehicular systems. However, it must be kept in mind that the available resolution of a radar system depends on the available bandwidth. Since the bandwidth of wi-fi signals is $B = 16.25\,\mathrm{MHz}$, the range resolution can never exceed $c_0/B \approx 18.25\mathrm{m}$, c_0 being the speed of light.

Using wi-fi signals for radar purposes has been suggested before; in [7], Falcone et al. propose the usage of such signals for bistatic passive radar. However, the setup proposed requires knowledge of the transmitted signal as well as additional signal processing to remove unwanted sidelobes. This raises the question if a true active radar system might be a viable option, which is what we discuss in this paper.

This paper is organized as follows: In Section II, we describe the setup of a system and describe how an IEEE 802.11a access point needs to be modified in order to also work as a radar station and elaborate on the radar algorithm. Section III will show simulations on how well this works, whereas Section IV shows some measurements to corroborate these results. Finally, Section V concludes.

II. System Description

Fig. 1 depicts the setup of such a wi-fi based radar station. It extends a regular access point by a radar subsystem, which consists of a digital radar processing unit and an analog receiver (the latter can be the same as the access point's own receiver if it is full-duplex capable). The radar subsystem is connected to the access point at two positions: first, it has access to any data transmitted by the access point; and second,

978-1-4673-1881-5/12/$31.00

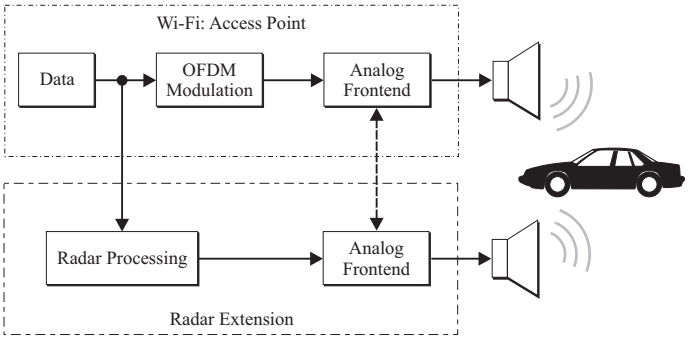

Fig. 1. A schematic of the wi-fi-based radar system

TABLE I
PARAMETERS OF THE OFDM SIGNAL RELEVANT TO THE RADAR PROCESSING

Value	Description
$\Delta f = 20\,\mathrm{MHz}/64 = 312.5\,\mathrm{kHz}$	Sub-carrier spacing
$T = 1/\Delta f = 3.2\,\mu\mathrm{s}$	Symbol duration
$T_G = 1/4T = 0.8\,\mu\mathrm{s}$	Guard interval duration
$T_O = T + T_G = 4\,\mu\mathrm{s}$	Total OFDM symbol duration
$N = 53$	Total number of carriers (including DC carrier)
$f_C = 5\,\mathrm{GHz}$	Centre frequency

the transmitting and receiving front-ends are synchronized to the same clock. This section will explain in detail how the radar subsystem works.

A. OFDM radar basics

In order to understand the algorithms used to obtain radar estimates, we will briefly discuss OFDM signals in radar scenarios. Table I lists the relevant physical parameters of the OFDM signals used in 802.11a systems. To simplify the analysis, we introduce the matrix notation for OFDM signals, where a transmitted frame is represented by a $N \times M$-matrix,

$$\mathbf{F}_{\mathrm{Tx}} = \begin{pmatrix} c_{0,0} & \cdots & c_{0,M-1} \\ c_{1,0} & \cdots & c_{1,M-1} \\ \vdots & \ddots & \vdots \\ c_{N-1,0} & \cdots & c_{N-1,M-1} \end{pmatrix} \in \mathbb{C}^{N\times M}. \quad (1)$$

Put simply, every row of the matrix corresponds to the data on one sub-carrier, whereas every column corresponds to the data on one OFDM symbol. The elements $c_{k,l}$ are symbols from a complex modulation alphabet (IEEE 802.11a allows several modulation alphabets depending on the link quality, ranging from BPSK up to 64-QAM). For wi-fi, the matrix has a total of 53 rows: 48 containing data, 4 containing pilot symbols and one empty DC carrier (at index $k = 26$). The number of OFDM symbols depends on the amount of data transmitted per packet. Preambles are not used for the radar imaging; the OFDM symbol at index $l = 0$ is thus the first OFDM symbol after the preamble, which means all modulation symbols $c_{k,l} \neq 0$ for $k \neq 26$.

Given some additional parameters, $\mathbf{F}_{\mathrm{Tx}}$ is equivalent to the transmitted signal. Converting the matrix into a transmitted signal is done by[1]

- running an IFFT of length 64 on every column,
- adding a cyclic prefix of length 16 samples,
- converting it to an analog signal at 20 MS/s and
- shifting it to the centre frequency f_C.

The system is configured such that the carrier with index 0 has the lowest frequency; therefore, the sub-carrier with the index k has the frequency $f_k = f_0 + k\Delta f$.

This matrix representation helps a lot when analyzing the effect of OFDM signals in a radar environment. Assume the radar signal is first transmitted, then it is reflected from an object at range r and relative velocity v_r and finally received. Since the receiver is synchronized with the transmitter, it is able to receive the signal exactly at the same time it is being transmitted. The received signal therefore is delayed by

$$\tau = 2r/c_0 \quad (2)$$

and shifted by a Doppler shift w.r.t. the transmit signal,

$$f_D = f_C \frac{v_r}{c_0}. \quad (3)$$

This has two distinct effects on the matrix: the delay causes a phase shift, which depends on the sub-carrier's frequency. The sub-carrier with index k therefore has a phase shift of $e^{2\pi j\tau(f_0+k\Delta f)}$. The Doppler shift causes a phase shift in time of $e^{2\pi j f_D T_O l}$. This becomes clear when we think of every sub-carrier as an individual, narrow-band digital signal with a symbol rate of T_O which is demodulated with a frequency offset of f_D.

Using this information, we can identify a received matrix $\mathbf{F}_{\mathrm{Rx}}$ corresponding to the transmitted matrix $\mathbf{F}_{\mathrm{Tx}}$. If a total of H reflections reach the receiver, each with an individual delay τ_h and a Doppler shift $f_{D,h}$, the received matrix has the form

$$(\mathbf{F}_{\mathrm{Rx}})_{k,l} = \sum_{h=0}^{H-1} (\mathbf{F}_{\mathrm{Tx}})_{k,l} \cdot b_h e^{j2\pi(lT_O f_{D,h} - k\tau_h\Delta f)} e^{j\varphi_h} + (\mathbf{W})_{k,l}. \quad (4)$$

This includes the receiver noise, which is modeled as additive white Gaussian noise (AWGN). Analogously to the transmit matrix, $\mathbf{F}_{\mathrm{Rx}}$ can be obtained from the received signal by analog/digital converting it at a sampling rate of $20\,\mathrm{MS/s}$, eliminating the cyclic prefix and processing every 64 samples with an FFT.

The phase term φ_h includes all random phase changes occurring on the channel as well as the phase change on the lowest frequency, $2\pi f_0 T_O$. Also present in (4) is the attenuation b_h, which depends on the distance of the reflecting target and its radar cross section (RCS). The matrix $\mathbf{W}$ contains random complex Gaussian variables, representing the AWGN.

As explained earlier, the radar processing unit has knowledge of the data transmitted. This allows a simple processing

[1] A full description of the modulation process can be found in [8].

step of $\mathbf{F}_{\text{Rx}}$ before performing any radar algorithms: We define a new matrix $\mathbf{F}$ as the element-wise quotient of $\mathbf{F}_{\text{Rx}}$ with the transmitted symbols,

$$(\mathbf{F})_{k,l} = \frac{(\mathbf{F}_{\text{Rx}})_{k,l}}{(\mathbf{F}_{\text{Tx}})_{k,l}} := \begin{cases} 0 \text{ if } k = 26 \\ e^{j(2\pi(lT_O f_{D,0} - k\tau_0 \Delta f) + \varphi_0)} + \frac{(\mathbf{W})_{k,l}}{(\mathbf{F}_{\text{Tx}})_{k,l}} \text{ otherwise.} \end{cases} \tag{5}$$

The DC carriers must be skipped to avoid a division-by-zero and are set to zero. Apart from these, the matrix $\mathbf{F}$ contains sinusoids only: one row- and one column-wise, respectively, for every target. This explains why the algorithms are called "spectral estimation based": the detection of targets as well as the estimation of their range and Doppler are equivalent to the identification of sinusoids in AWGN.

B. Signal requirements

As explained in [9], the OFDM signal must fulfill certain requirements for (5) to be correct. Specifically, de-orthogonalisation must be avoided to make sure the elements of $\mathbf{F}_{\text{Rx}}$ are correctly aligned to the corresponding ones of $\mathbf{F}_{\text{Tx}}$.

First, τ must be smaller than T_G, which corresponds to a maximum target distance of $240\,\text{m}$. Also, the maximum Doppler shift must stay much smaller than the sub-carrier spacing. Even at a relative velocity of $200\,\text{km/h}$, the Doppler shift is approx. $1\,\text{kHz} \ll \Delta f$, so this is no problem. Also, the Doppler shift must be considered constant over all sub-carriers. For the same maximum relative velocity, the difference in Doppler shift between that on carrier 0 and carrier 52 is approx. $20\,\text{Hz}$, or approx. 2% of the total Doppler shift.

For distances smaller than $240\,\text{m}$ and relative velocities smaller than $200\,\text{km/h}$ thus all signal requirements are considered fulfilled.

C. Periodogram-based algorithms

For the one-dimensional case of detecting sinusoids in discrete-time, time-limited signals, the periodogram has been proven to be a good, in some cases even optimal solution [10, Chap. 13]. A two-dimensional periodogram was therefore proposed as the core element of OFDM radar algorithms [3, Section IV]; it is defined as

$$\text{Per}_{\mathbf{F}}(n,m) = \frac{1}{NM} \left| \underbrace{\sum_{k=0}^{N_{\text{Per}}-1} \overbrace{\left(\sum_{l=0}^{M_{\text{Per}}-1} (\mathbf{F})_{k,l} e^{-j2\pi \frac{lm}{M_{\text{Per}}}} \right)}^{\text{FFT of length } M_{\text{Per}}} e^{j2\pi \frac{kn}{N_{\text{Per}}}}}_{\text{IFFT of length } N_{\text{Per}}} \right|^2. \tag{6}$$

Apart from the extension to two dimensions, this differs from the classical periodogram in two respects:

- The vertical dimension (index k) has a positive sign to match the corresponding sinusoid $e^{-k\tau\Delta f}$.
- The periodogram is quantized to a total of $N_{\text{Per}} \times M_{\text{Per}}$ points. While this produces a quantization error, it also allows the periodogram to be efficiently be calculated by FFTs and IFFTs, as indicated in (6).

To suppress sidelobes, it makes sense to multiply $\mathbf{F}$ element-wise with a window matrix $\mathbf{W} \in \mathbb{C}^{N \times M}$. For the remainder of this paper, we use a Hamming window matrix $\mathbf{W} = w_N^T(k) \otimes w_M(l)$, where $w_N(k)$ is a row vector of length N containing a one-dimensional Hamming window and $\otimes$ denotes the dyadic product.

Using the periodogram, an OFDM radar algorithm consists of the following steps:

1) Obtain the matrix $\mathbf{F}$ from the input samples
2) Calculate the periodogram (6)
3) Find the peak points in $\text{Per}(n,m)$
4) A peak at $\hat{n}, \hat{m}$ corresponds to a target at

$$\hat{d} = \frac{\hat{n} c_0}{2\Delta f N_{\text{Per}}} \quad \text{and} \quad \hat{v} = \frac{\hat{m} c_0}{2 f_C T_O M_{\text{Per}}}. \tag{7}$$

Additional measures can be taken to interpolate the true value of $\hat{d}$ and $\hat{v}_r$ between integer values of m and n, but this will not be discussed in this paper.

D. DC carrier influence

As mentioned before, the DC carrier ($k = 26$) is left empty, and it must be understood how this affects the periodogram. Since this effect only occurs in one dimension, consider the following analysis: Assume $x(k) = w(k) e^{j2\pi k \tau \Delta f} e^{j\varphi}, k = 0 \ldots 52$ a one-dimensional sinusoid with random phase and window function $w(k)$. A periodogram of the same sinusoid lacking a sample at index $k = 26$ has the form

$$\text{Per}(n) = \left| \sum_{k=0}^{52} (x(k) - \delta(k-26) e^{j2\pi 26 \tau \Delta f}) e^{j2\pi \frac{kn}{N_{\text{Per}}}} \right|^2 \tag{8}$$

$$= \text{Per}_{x(k)}(n) + \frac{1}{53} - \frac{2}{53} \sum_{k=0}^{52} w(k) \cos\left((2\pi(k-26)(\tau\Delta f + \frac{n}{N_{\text{Per}}}) \right). \tag{9}$$

The first summand in (9) is equal to the periodogram of $x(k)$, which shows that the basic shape of the periodogram is not changed. The two other summands produce spurious elements in the periodogram, which increase the energy levels outside of the main lobe. In simulations, we perceive a $27\,\text{dB}$ peak-to-spur ratio, the same as in [7]. This value stems from the fact that the last two summands produces a spur level oscillating around $0\,\text{dB}$, whereas the peak of the Hamming window in the same normalization is at $27\,\text{dB}$.

E. Multi-target detection

Up until now, the periodogram was not processed further to automatically detect the exact position of targets. In the following, we use a very simple algorithm, dubbed *successive target cancellation* (STC), which requires a value for the false alarm rate P_f and an estimate of the noise power σ^2. It consists of the following steps:

1) Calculate a threshold value γ from the noise power and the false alarm rate by

$$\gamma = \sigma^2 \cdot F_{\chi_2^2}^{-1}(\sqrt[\frac{1}{MN}]{1 - p_F}), \tag{10}$$

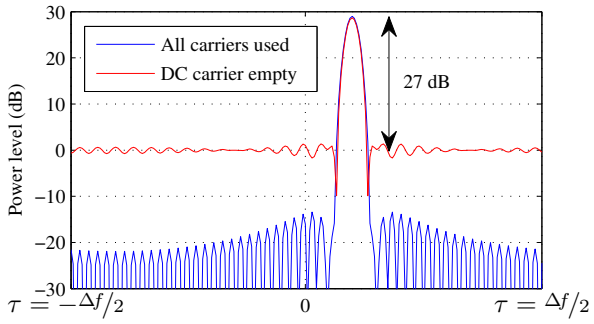

Fig. 2. Periodogram of a length-53 sinusoid with and without an active DC carrier

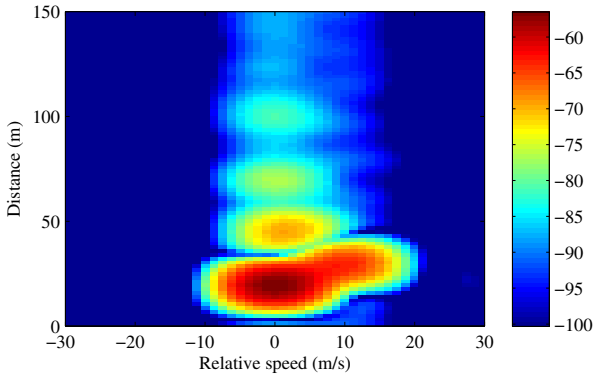

Fig. 3. Periodogram during the simulation, target distance 30 m

where $F_{\chi^2_2}^{-1}$ is the inverse CDF of χ^2_2-distribution which describes the noise in the periodogram.

2) Find $\hat{n}, \hat{m} = \arg\max_{n,m} \mathrm{Per}(m,n)$. If $\mathrm{Per}(\hat{n},\hat{m}) < \gamma$, quit.
3) If this target is less than the size of one main lobe apart from a previous target or if there is another target with the same Doppler and more than 27 dB more power, ignore it. Otherwise, use (7) to calculate the estimated range and Doppler. Add this to list of targets.
4) Remove the components of the current target from $\mathbf{F}$ using the following subtraction:

$$(\hat{\mathbf{F}})_{k,l} = (\hat{\mathbf{F}})_{k,l} - \mathbf{F}_{\hat{n},\hat{m}} e^{j2\pi\left(\frac{l\hat{m}}{M_{\mathrm{Per}}} - \frac{k\hat{n}}{N_{\mathrm{Per}}}\right)} w_N(k) w_M(l). \tag{11}$$

5) Repeat from step 2) until loop terminates.

If the noise power is not know a-priori, it can be estimated from the periodogram by calculating the mean of all periodogram values at a very far distance, based on the assumption that no valid target will cause a peak at this position. The value for the noise power is then

$$\hat{\sigma}^2 = \frac{1}{M_{\mathrm{Per}}} \sum_{m=0}^{M_{\mathrm{Per}}} \mathrm{Per}_{\mathbf{F}}(N_{\mathrm{Per}}, m). \tag{12}$$

III. Simulations

Simulations were done to verify the system. For every simulated measurement, a signal with the properties from Table I was created. A list of targets was passed to the simulator, which then calculated the received signal by delaying, Doppler-shifting and attenuating the signal accordingly. AWGN was then added with a noise power density of $N_0 = k_B T \cdot \mathrm{NF}$, where k_B is the Boltzmann constant, $T = 290\,\mathrm{K}$ the noise temperature and $\mathrm{NF} = 20\,\mathrm{dB}$ the noise figure. Attenuation was calculated by the point-scatter model, such that the received power from a target at range r and with RCS σ_{RCS} is

$$P_{\mathrm{Rx}} = P_{\mathrm{Tx}} \frac{c_0 G \sigma_{\mathrm{RCS}}}{(4\pi)^3 r^4 f_C^2}. \tag{13}$$

Transmit power in the simulations was set to $P_{\mathrm{Tx}} = 20\,\mathrm{dBm}$. G is an optional antenna gain which was set to 10 dB. We used a total of $M = 3072$ OFDM symbols, as this was used for the measurements. All targets had the same RCS of $10\,\mathrm{dBm}^2$.

The STC algorithm was parametrized with a desired false alarm rate of $P_f = 0.1$. Noise power was estimated using (12).

The first simulation consisted of three stationary clutter objects at ranges 20, 70 and 100 m, one moving clutter object at $r = 45\,\mathrm{m}$ with a relative velocity of $v_r = 2\,\mathrm{m/s}$ and one target with a relative velocity of $v_r = 10\,\mathrm{m/s}$. The latter target's range was changed from 150 m to 15 m in steps of 5 m. At every position of the target, 200 simulated measurements were performed, yielding the following results:

- The false alarm rate was slightly lower than intended ($P_f = 0.05$). The main reason is that the noise estimation (12) does not account for spurs caused by the missing DC carrier and will thus overestimate the noise power.
- The detection rate with the given setup was 100%. The root mean square error for the range of the objects was $0.5957\,\mathrm{m}$, for the relative velocity it was $0.0454\,\mathrm{m/s}$.

Fig. 3 shows a periodogram during the simulation. Anything below the threshold γ is not shown. The spurs caused by the missing DC carrier can be clearly seen.

These results are quite encouraging, but it is clear that the scenario was chosen such that the objects were quite far apart in the range/Doppler plane, thus not posing any problems related to limited resolution. Further simulations were run to determine a practical resolution of this method, in which two targets with identical Doppler were moved towards each other to obtain a value for the range resolution. The simulations suggest the targets must be at least 20 m apart to correctly identify them both. In a similar fashion, simulations with two targets at the same range, but differing relative velocities were performed, and show that the targets must have a difference in velocities of at least $6\,\mathrm{m/s}$ to be distinguished properly.

However, the STC algorithm performs poorly for a multitude of close targets. Other algorithms, such as RELAX [11], exist which will be investigated to increase detection performance.

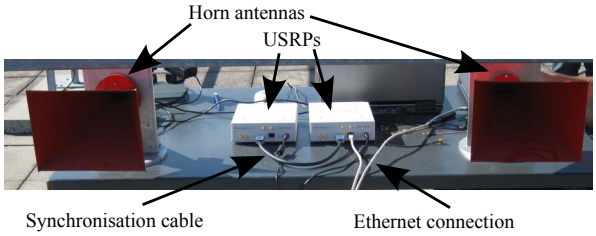

Fig. 4. The measurement setup. The right-hand USRP is connected to a laptop (not shown).

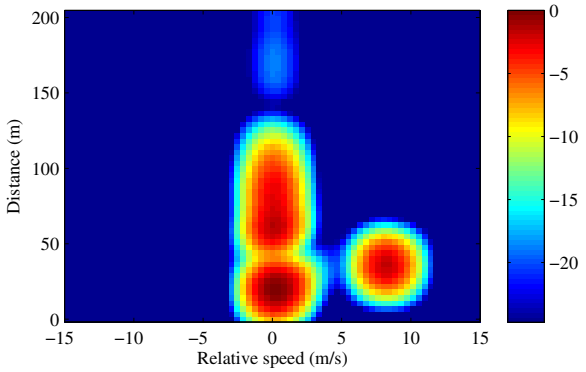

Fig. 5. Periodogram output of the measurement. The moving target is correctly identified.

IV. Measurements

In order to confirm the simulations, some measurements were performed. The measurement setup, depicted in Fig. 4 consisted of two universal software radio peripherals (USRP) N210 by Ettus Research LLC. The USRPs were connected by a MIMO cable, which we used to synchronize the clocks and also transfer data between terminals. This allows controlling both USRPs with one laptop. We use Matlab to create the transmit signal and for the signal processing on the received signal. Custom software developed for this task is used to first synchronize the clocks, and then start a synchronous transmit/receive on the two USRPs.

Horn antennas with a high directivity were used for both the transmitter and the receiver (in the more practical case where the wi-fi access point would also be used to provide data access, the transmit antenna would most likely be omnidirectional; however, for these measurements, a directive antenna was chosen to reduce the coupling between antennas).

The signals were parametrized as in Table I, with two modifications: for a useful Doppler resolution, we transmitted $M = 3072$ OFDM symbols per frame. 802.11a specifies a maximum number of 4095 bytes per frame, which, at the lowest bit rate, corresponds to a maximum number of 1365 OFDM symbols per frame. This means at least three consecutive packets would have to be sent in order to achieve the same Doppler resolution.

Also, the centre frequency was increased to $5.9\,\mathrm{GHz}$ because the available antennas had too high attenuation at the regular frequency of $5\,\mathrm{GHz}$.

Fig. 5 shows a periodogram of the measurement, normalized to the largest peak. The STC algorithm identifies the moving target correctly, but also identifies three stationary clutter objects at $22\,\mathrm{m}$, $92\,\mathrm{m}$ and $144\,\mathrm{m}$, again showing the deficiencies of the STC algorithm. Note that the total dynamic range of this periodogram is much smaller than that in Fig. 3, which is why the DC carrier-related spurs do not show up as prominently.

V. Conclusion

By simulation and measurements, we could show that wi-fi based OFDM radar can work and does not even require complex signal processing if the transmit data is available at the receiver. This opens up new possibilities for "pseudo-passive" radar systems (which are actually active radar systems, but use data transmission signals which are sent anyway). This is an easy way to include radar sensors into OFDM transmitters simply by adding a receiver path, without any additional spectrum usage.

Of course, in such systems, bandwidth and signal duration (which determine range and Doppler resolution, respectively) cannot be freely chosen and often lead to sub-optimal resolution. If the available resolution is sufficient, though, this is a clearly a good way to create additional radar imaging sensors.

References

[1] C. Sturm, T. Zwick, and W. Wiesbeck, "An OFDM System Concept for Joint Radar and Communications Operations," *Vehicular Technology Conference, 2009. 69th IEEE*, April 2009.

[2] C. Sturm, E. Pancera, T. Zwick, and W. Wiesbeck, "A Novel Approach to OFDM Radar Processing," *Radar Conference, IEEE*, May 2009.

[3] C. Sturm and W. Wiesbeck, "Waveform Design and Signal Processing Aspects for Fusion of Wireless Communications and Radar Sensing," *Proceedings of the IEEE*, vol. 99, no. 7, pp. 1236 –1259, July 2011.

[4] B. Donnet and I. Longstaff, "Combining MIMO Radar with OFDM Communications," *Radar Conference, 2006. EuRAD 2006. 3rd European*, pp. 37–40, Sept. 2006.

[5] M. Braun, C. Sturm, A. Niethammer, and F. K. Jondral, "Parametrization of Joint OFDM-based Radar and Communication Systems for Vehicular Applications," *20th IEEE Symposium on Personal Indoor and Mobile Radio Communications*, 2009.

[6] M. Braun, Y. Koch, C. Sturm, and F. K. Jondral, "Signal Design and Coding for High-Bandwidth OFDM in Car-to-Car Communications," *Vehicular Technology Conference, 2010. 72nd IEEE*, September 2010.

[7] P. Falcone, F. Colone, C. Bongioanni, and P. Lombardo, "Experimental results for OFDM WiFi-based passive bistatic radar," in *Radar Conference, 2010 IEEE*, May 2010.

[8] *IEEE 802.11 Standard, Part 11*, 2005.

[9] M. Braun, C. Sturm, and F. K. Jondral, "Maximum Likelihood Speed and Distance Estimation for OFDM Radar," *Radar Conference, IEEE International*, 2010.

[10] S. M. Kay, *Modern Spectral Estimation*. Prentice Hall, 1988.

[11] J. Li and P. Stoica, "Efficient mixed-spectrum estimation with applications to target feature extraction," *Signal Processing, IEEE Transactions on*, vol. 44, no. 2, pp. 281 –295, Feb 1996.